J. Fluid Mech. (1985), *vol.* 150, *pp.* 23–39
Printed in Great Britain

Large-scale structures in a forced turbulent mixing layer

By M. GASTER†, E. KIT AND I. WYGNANSKI
Faculty of Engineering, Tel-Aviv University

(Received 15 November 1982 and in revised form 19 June 1984)

The large-scale structures that occur in a forced turbulent mixing layer at moderately high Reynolds numbers have been modelled by linear inviscid stability theory incorporating first-order corrections for slow spatial variations of the mean flow. The perturbation stream function for a spatially growing time-periodic travelling wave has been numerically evaluated for the measured linearly diverging mean flow. In an accompanying experiment periodic oscillations were imposed on the turbulent mixing layer by the motion of a small flap at the trailing edge of the splitter plate that separated the two uniform streams of different velocity. The results of the numerical computations are compared with experimental measurements.

When the comparison between experimental data and the computational model was made on a purely local basis, agreement in both the amplitude and phase distribution across the mixing layer was excellent. Comparisons on a global scale revealed, not unexpectedly, less good accuracy in predicting the overall amplification.

1. Introduction

High-Reynolds-number flows are generally dominated by broadband velocity fluctuations. Although this so-called 'turbulence' is often treated as a random process through various averaged statistical quantities, it does seem that there can be some degree of order buried within the apparent chaos. Flow visualization has shown that large-scale (low-frequency) oscillations occur in certain types of flow in the form of travelling waves, whilst in other flows it seems that discrete large-scale isolated 'events' develop. Wavelike behaviour is most prevalent in unbounded flows, like jets, wakes or free mixing layers. These flows are especially sensitive to external excitation, or 'forcing'. Even very weak external disturbances can influence the flow markedly; the developing unsteady wave motion inevitably reflects the level and character of the natural disturbances in the flow.

The travelling-wave structures that can be seen so clearly in some flow visualizations of *turbulent* jets or mixing layers are quite similar to those seen in *laminar* jets or mixing layers. This similarity between the patterns in laminar and turbulent states is not very surprising in view of the fact that the basic long-wave vorticity-transport instability mechanism is mainly controlled by the mean-velocity profiles of the flow, and these are not too different in the two situations. The roll-up process that can be seen in smoke or dye patterns in laminar flows can be explained in terms of an instability of the mean flow, and a linear calculation is often capable of providing a reasonably good estimate of the initial development of this process (Michalke 1965). The notion that a turbulent flow, even though it contains a fine-scale structure, is

† Permanent address: National Maritime Institute, Teddington, Middlesex, U.K.

also unstable in the above sense is not at all new (see e.g. Malkus 1956; Landahl 1967; Liu & Merkine 1975; Hussain & Reynolds 1970). The fine-scale turbulence provides additional mixing on a small scale and behaves like an added 'eddy' viscosity on the mean and large-scale motions. As viscosity is in any case not of primary importance in these inviscidly unstable free shear flows, it seems that the fine-scale turbulence plays no significant role in the development of the large-scale motion. This decoupling of the fine-scale turbulence from the large structures enables classical stability theory for laminar flows to be applied to certain types of turbulent motion.

It is convenient to study instabilities experimentally through the introduction of known controlled disturbances. This has commonly been done in experiments on laminar flows by direct mechanical devices, like the vibrating ribbon used by Schubauer & Skramstad (1947), or by acoustic excitation (Freymuth 1966). Artificial excitation by some form of periodic forcing, at the nozzle or lip where the separated shear layers form, creates an isolated wavetrain that can be related to a spatial eigenmode of the equations of motion. Broadband excitation, occurring with high levels of free-stream turbulence, creates a modulated wavetrain composed of many modes. Although the artificially triggered periodic wavetrain is a gross oversimplification of the broadband motion that occurs in most physical flows, its study will hopefully provide a basis on which to build a more representative model of the large-scale structures that are observed in the unforced case.

Here we are concerned with the behaviour of a periodically forced turbulent mixing layer (Oster & Wygnanski 1983). The laboratory mixing layer was formed downstream of a splitter plate separating two uniform streams of different velocities issuing from a specially constructed open-return wind tunnel. A small flap hinged at the trailing edge of the splitter plate was driven at a given frequency so as to introduce a controlled periodic oscillation into the mixing layer. Experiments similar to that described in this paper have previously been carried out on a laminar shear layer excited by an acoustic source. Data from that extensive set of measurements (Freymuth 1966) have been compared with the linear stability calculations of Michalke (1964, 1965) for both temporal and spatial modes. Freymuth's measurements of local growth rates and wave speeds correlated rather more closely with those derived from the spatial theory than those calculated from the temporal model via a space–time transformation. More detailed comparisons of the eigenfunctions with the measured distributions of velocity fluctuations across the flow provided positive support for the spatial representation. Temporal modes, although convenient as far as computations are concerned, do not properly describe the oscillatory flows that actually occur in experiment.

The Rayleigh equations, which were used by Michalke for the determination of eigenvalues and eigenmodes, are obtained by linearization of the inviscid disturbance equations for a parallel mean flow. The assumption of a parallel base flow enables the equations to be separated in Cartesian coordinates, and the modal decomposition can then be accomplished through the solution of ordinary differential equations. In some flows the use of parallel-flow approximation is untenable and it is necessary to obtain solutions of the partial differential equations that describe the disturbance more completely. Provided that the mean flow deviates from a parallel flow sufficiently slowly, approximate solutions to the partial differential equations can be obtained in terms of scaled solutions of the 'locally parallel-flow' stability problem, and again this only requires the integration of ordinary differential equations. The scaling function can be obtained by a multiple-scale expansion in terms of a suitable small parameter defining the slow variation of the mean-flow velocity profile with

the streamwise coordinate. Alternatively, an iteration scheme can be devised to generate a correction series to the locally parallel-flow solution (see Gaster 1974).

Bouthier (1972, 1973) used the multiple-scale technique to provide a more consistent, and (it is to be hoped) more accurate, analysis of spatially growing waves in the laminar boundary layer of a flat plate. The first-order correction to the Orr–Sommerfeld solution certainly improved correlation between experiment and theory, but some discrepancies remain. The flat-plate boundary layer deviates from a parallel flow only very slowly, and it is perhaps not surprising that the correction to the amplification rates in this case is hardly significant. Corrections become more important in flows like jets and mixing layers that spread rapidly. Crighton & Gaster (1976) computed growth rates and phase speeds of the large-scale turbulent structures in an axisymmetric jet, taking the effect of spatial growth into account, and obtained encouraging agreement with the experimental data of Crow & Champagne (1970). In these computations the first-order corrections to wave speed and amplification rates turned out to be significant.

The large-scale structures that occur in a turbulent mixing layer have also been studied experimentally by many authors (Ho 1981; Fiedler *et al.* 1981), and some of the data have been compared with predictions based on laminar stability theory. Much of this work has been carried out on the mixing layer between two *moving* streams. Although the shape of the resulting velocity profile has been shown to be reasonably close to the 'tanh' profile used by Michalke in his calculations of the stability of the laminar flow where one of the streams was stationary, there is an additional translational velocity component superimposed on the mean flow when both streams are moving (i.e. when the velocity ratio is non-zero). Fiedler *et al.* (1981) achieved some success in linking Michalke's data gathered from a forced mixing layer, but in their case the velocity ratio was zero, and the comparison with spatial theory was straightforward. The velocity ratio turns out to have a sizeable effect on both the shapes of the spatial eigenfunctions and on the eigenvalues themselves, as recently demonstrated by Monkewitz & Huerre (1982). Thus, although qualitatively the temporal instability model can be used as a rough guide of the local growth rates and phase speeds, the detailed overall picture of the evolution of waves in a mixing layer obtained in this manner is likely to compare poorly with experiment (Oster & Wygnanski 1983).

In this paper we relate the flow-field measurements obtained in a forced turbulent mixing layer to predictions based on linearized theory that is scaled to account for slow mean-flow divergence. The velocity fluctuations were recorded for various stream velocities and velocity ratios, at different frequencies and levels of excitation. The amplitude of the flap oscillations was kept small so that linearized theory would be applicable, at least in the initial region of growth. It was found that the mean flow was only slightly influenced by the imposed excitation. A similarity mean-flow structure was obtained, with the velocity profile close to the 'tanh' shape used in previous calculations. The thickness of the shear layer was found to increase almost linearly with distance downstream from some virtual origin near the trailing edge of the flap. The locally parallel flow eigenvalues and eigenfunctions were used in an expansion scheme to obtain first-order corrections for the effects of flow divergence. The resulting predictions of the velocity fluctuations throughout the region supporting unstable wavetrains are compared with phase-averaged measurements of the forced turbulent flow.

2. Analysis

An approximate solution of the equations defining the propagation of small-amplitude wavy disturbances is sought for the slow diverging mixing-layer flow. Viscosity has virtually no effect on the behaviour of the highly amplified waves that arise in these flows, and consequently the viscous terms will be neglected.

We apply the method used by Crighton & Gaster (1976) to the two-dimensional mixing layer so as to generate a first-order correction to the quasi-parallel-flow perturbation stream function in the form

$$\hat{\psi}(\xi,\eta,t) = A(\xi)\,\phi(\xi,\eta)\exp\left\{\mathrm{i}\left(\int_{\xi_0}^{\xi_1}\alpha(\xi)\,\mathrm{d}\xi-\omega t\right)\right\}, \tag{2.1}$$

where ξ and η are non-dimensional coordinates in the free-stream and normal directions, linked to the physical quantities x and y through the chosen scale $L = (\bar{U}_2-\bar{U}_1)\,C_0/2\pi f$, in which $\bar{U}_1$ and $\bar{U}_2$ are the velocities of the faster and slower streams respectively, f is the excitation frequency and C_0 is a constant equal to a dimensionless ω, and t is dimensionless time. Therefore $\eta = y/L$ and $\xi = C_1 x/L$; the numerical values of C_0 and C_1 will be determined later.

The function $A(\xi)$ is defined by

$$A(\xi)\,N(\xi)+\frac{\mathrm{d}A}{\mathrm{d}\xi}(\xi)\,M(\xi) = 0, \tag{2.2}$$

where

$$N(\xi) = \int_{-\infty}^{+\infty}\left\{\omega\left[\phi_0\frac{\partial\alpha}{\partial\xi}+2\alpha\frac{\partial\phi_0}{\partial\xi}\right]+\bar{U}\left[\frac{\partial\phi_0''}{\partial\xi}-3\alpha^2\frac{\partial\phi_0}{\partial\xi}-3\alpha\phi_0\frac{\partial\alpha}{\partial\xi}\right]\right.$$
$$\left.+\phi_0'\frac{\partial}{\partial\xi}(\bar{U}')-\bar{U}''\frac{\partial\phi_0}{\partial\xi}+\bar{V}[\phi_0'''-\alpha^2\phi_0']\right\}\bar{\phi}_0\,\mathrm{d}\eta$$

and

$$M(\xi) = \int_{-\infty}^{+\infty}\{2\alpha\omega\phi_0+\bar{U}[\phi_0''-3\alpha^2\phi_0]-\bar{U}''\phi_0\}\,\bar{\phi}_0\,\mathrm{d}\eta.$$

In these expressions $\phi_0(\xi,\eta)$ is the 'local' eigenfunction obtained from the Rayleigh equation

$$\left(\bar{U}(\xi,\eta)-\frac{\omega}{\alpha}\right)(\phi_0''-\alpha^2\phi_0)-\bar{U}''(\xi,\eta)\,\phi_0 = 0 \tag{2.3}$$

and $\bar{\phi}_0$ is the adjoint eigenfunction. Note that, at any streamwise location ξ, only the η-dependences of $\bar{U}$, $\bar{U}'$ and $\bar{U}''$ are needed. Consequently for a given excitation frequency the eigenvalue α is defined as a function of ξ only.

3. Computation

The mean flow was assumed to have a similar velocity profile throughout the computational region, extending from the virtual origin of the flow ($\xi = 0$), to a position downstream ($\xi = 1$) where linear amplification of the excited wave ceased (i.e. $\alpha_1 = 0$). The chosen velocity profile family was of the form

$$\frac{\bar{U}-\bar{U}_1}{\bar{U}_2-\bar{U}_1} = \frac{1}{2}\left[1+F\left(\frac{\eta}{\xi}\right)\right], \tag{3.1}$$

where $\bar{U}$ is the local mean velocity. Michalke considered a parallel flow independent of x for the case $U_1 = 0$ and represented F by $\tanh\eta$. Initial computations were made

on this profile shape in order to check our numerical procedures for finding the eigenvalues and eigenfunctions, but most of the numerical results presented here were obtained with the more appropriate velocity function given later in (5.2).

A rectangular computational zone extending from $\xi = 0.082$ to $\xi = 1$ in the stream direction, and from $\eta = -1.5$ to $\eta = 1.5$† across the flow was used. 50 intervals ($\Delta\xi = 0.018$) were generally taken in the stream direction and 400 were used across the flow. The prediction of the wavetrain to lowest order required the solution of the ordinary differential equations defining the local structure (2.3), as well as the evaluation of the integrals in (2.2) that provide the amplitude scaling $A(\xi)$.

It was found that specifying the constant C_0 in the definition of L as†

$$C_0 = \frac{2\pi f L}{\bar{U}_2 - \bar{U}_1} = \frac{0.7}{\lambda} = \omega, \tag{3.2}$$

where

$$\lambda = \frac{\bar{U}_2 - \bar{U}_1}{\bar{U}_2 + \bar{U}_1},$$

provided a neutrally amplified mode at the end of this computational domain ($\xi = 1$). This relates the normalizing lengthscale L to the physical frequency and velocity difference. For this frequency the eigenvalues $\alpha(\xi)$ and the eigenfunctions $\phi(\xi, \eta)$ were evaluated at each of the streamwise locations. The eigensolutions were obtained by a standard shooting technique that used a 4th-order Runge–Kutta procedure to integrate (2.3) from one boundary to another. Iteration on $\alpha(\xi)$ was carried out until solutions compatible with the necessary exponential decay both above and below the mixing layer were obtained.

These solutions $\phi_0(\xi, \eta)$ with their derivatives $\phi_0'(x, h)$ and ϕ_0'' etc. were stored on disc, together with the adjoint function $\bar{\phi}_0(\xi, \eta)$, which was evaluated in a similar way from the differential equation adjoint to (2.3). A second program used these stored solutions to evaluate the integrals N and M, across the flow field. In the computation of M and N it was necessary to form derivatives of $\alpha(\xi)$, $\bar{u}(\xi, \eta)$, $\bar{u}'(\xi, \eta)$, $\bar{u}''(\xi, \eta)$, $\phi_0(\xi, \eta)$, etc. with respect to ξ by differencing neighbouring sets of data. A further program then introduced the necessary mean-flow divergence $\mathrm{d}\theta/\mathrm{d}x$ (defined in (5.1)) and finally evaluated the amplitude scaling function.

4. Experiments

Measurements of both mean and fluctuating velocities were made in a periodically forced turbulent mixing layer that formed downstream of a splitter plate separating two streams of different velocities. A detailed description of the wind tunnel and experimental procedure is given by Oster & Wygnanski (1983).

Two-dimensional sinusoidal oscillations of small amplitude were generated in the flow by the motion of a thin flap of 1 cm chord hinged to the trailing edge of the splitter plate. The flap was actuated by an electromagnetic driver fed by an electronic signal generator. During the experiment a theodolite was used to monitor the flap motion under stroboscopic illumination in order to ensure that the amplitude remained constant.

A 10-element rake of hot-wire probes was used to survey the shear layer. The rake was mounted on a carriage that could be traversed in directions both normal and

† For the 'tanh' velocity profile the computational range extended from -3 to $+3$, and $C_0 = 0.5/\lambda$.

parallel to the flow. Typically 2–3 transverse locations were used in the normal direction at a given streamwise position so as to provide between 20 and 30 measuring points across the shear layer. The voltages generated by the hot-wire anemometers were digitized to 12 bit resolution and written on a magnetic tape. Most of the measurements reported were made at downstream distances of between 200 mm and 1000 mm from the flap trailing edge, covering approximately 5 wavelengths for the data in set I.

Three sets of experimental data were acquired. For each set the velocities of the two streams forming the mixing layer, the frequency and amplitude of the flap oscillation were kept constant. Each set of data contained measurements from some 20 streamwise locations.

At each station the mean-velocity profiles were obtained by averaging the velocity records in a conventional manner, using the computer to linearize the raw hot-wire anemometer data. The digital records from each measuring point were also processed on the computer to provide the fundamental component of the signal that was phase-locked to the flap motion. The records were phase-averaged over 200 sample blocks, each of which was equivalent to a single cycle of the flap motion. The Fourier transform of these averaged records then provided the phase and amplitude estimates of the spectral elements of the velocity field largely free from the random turbulence present in the original signals.

5. Results

The growth rate of the mixing layer with increasing downstream distance is most conveniently expressed by

$$\frac{\mathrm{d}\theta}{\mathrm{d}x} = \frac{\mathrm{d}}{\mathrm{d}x}\int_{-\infty}^{+\infty} \frac{\bar{U}-\bar{U}_1}{\bar{U}_2-\bar{U}_1}\left[1-\frac{\bar{U}-\bar{U}_1}{\bar{U}_2-\bar{U}_1}\right]\mathrm{d}y. \tag{5.1}$$

The variation of θ with distance from the trailing edge of the splitter plate is shown in figure 1 for each of the three data sets. The measured momentum thickness increases almost linearly from some origin near the flap at a rate that depends on the velocities of the two streams and to some extent on the level and frequency of the excitation (see also Oster & Wygnanski 1983). The rate of spread of the mixing layers is given by the slopes of these lines. In each case $\mathrm{d}\theta/\mathrm{d}x \ll 1$, which is entirely consistent with the assumption of slow divergence that was made in the analytical treatment of the flow stability.

Some important mean-flow parameters governing each data set are given in table 1, in which a_f is the amplitude of the flap oscillation and x_0 is the virtual origin at which $\theta = 0$.

The mean-flow velocity profiles are plotted on figure 2 in similarity variables. A very good collapse is evident, but the resultant mean does not fall on the 'tanh' profile shape that has so often been used to describe the flow of mixing layers. A polynomial fit based on the 'tanh' profile and its derivatives was found to provide a better fit to the data:†

$$\frac{\bar{U}-\bar{U}_1}{\bar{U}_2-\bar{U}_1} = 0.5\left[1+\left(1+0.67\,\mathrm{sech}^2\frac{\eta}{\xi}\right)\tanh\frac{\eta}{\xi}\right], \tag{5.2}$$

† This form was suggested by Dr. R. E. Kaplan, from the University of Southern California.

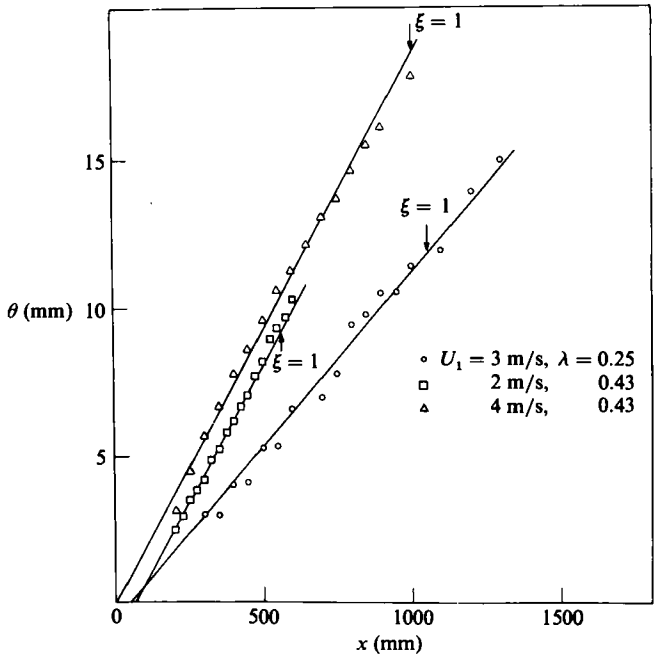

FIGURE 1. The variation of the momentum thickness with distance from the trailing edge.

Set	$\overline{U}_1$ (m/s)	$\overline{U}_2$ (m/s)	λ	$\frac{dx}{d\theta}$	x_0 (mm)	f (Hz)	a_f (mm)
I	3	5	0.25	85	50	20	0.5
II	2	5	0.43	54	60	20	0.5
III	4	10	0.43	54	0	20	1.0

TABLE 1

where the transverse distance y in the definition of η was measured from the location at which $(\overline{U}-\overline{U}_1)/(\overline{U}_2-\overline{U}_1) = 0.5$. Substituting (5.2) into (5.1) yields

$$\frac{d\theta}{dx} = 0.2467C_1, \tag{5.3}$$

and therefore the constant C_1 is linked to the physical rate of spread of the mixing layer by $C_1 = (d\theta/dx)/0.2467$, making

$$\xi = \frac{(x-x_0)\,d\theta/dx}{0.2467L}$$

and

$$\frac{\eta}{\xi} = \frac{0.2467(y-y_{0.5})}{\theta},$$

where θ is the local momentum thickness defined by (5.1). It is interesting to note that on the high-velocity side of the flow the local mean velocity can exceed $\overline{U}_2$ by approximately 1 %, resulting in $d\overline{U}/d\eta < 0$ near the edge of the shear layer.

We now turn our attention to the fluctuating components of the flow. The

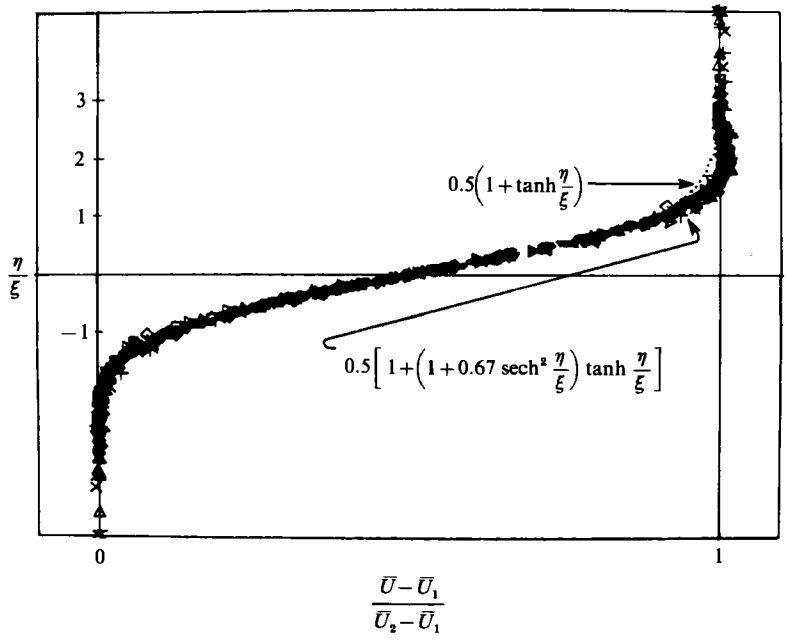

FIGURE 2. The mean-velocity distribution in a plane turbulent mixing layer.

amplitude of the fundamental component of the artificially excited wavetrain at each streamwise station can be defined in terms of the integral of the modulus of the fluctuating velocity u' evaluated across the mixing layer

$$\int_{-\infty}^{\infty} |u'|\,\mathrm{d}y. \tag{5.4}$$

Measured amplitudes defined in this way are plotted on figure 3 together with the results of the numerical computations for the theoretical model. Since the computed and the measured integral values were normalized with respect to the first reference x-location at which the mean flow was self-similar, figure 3 represents a measure of overall amplification; this was approximately equal to 4 for data sets I and II, and 9 for data set III. Theoretical amplifications are also presented on this figure for the modified mean-velocity profiles, and in one instance for the 'tanh' profile as well. Correlation between calculated and experimental growth is not very good, although it is quite reasonable in view of all the assumptions and approximations made in formulating the mathematical model. The choice of mean-flow velocity profile clearly affects the calculated amplification rates (figure 3, set III) and, as we shall see later, also the shape of the local eigenfunction. The different amplification patterns shown on figure 3 give some indication of the effect of small variations in the mean-velocity profile. The modified profile shape given by (5.2) was found to fit the experimental data better, and all further numerical results reported here are based on that family.

Figure 4 shows a comparison between measured and computed phase angles along 3 different rays (y_1 corresponds to the locations at which $(\bar{U}-\bar{U}_1)/(\bar{U}_2-\bar{U}_1)\to 1$; $y_{\frac{1}{2}}$ corresponds to $(\bar{U}-\bar{U}_1)/(\bar{U}_2-\bar{U}_1)=0.5$, and the value of $(\bar{U}-\bar{U}_1)/(\bar{U}_2-\bar{U}_1)$ at y_0 approaches 0). The phase clearly advances more rapidly in the faster-flowing regions, a trend modelled by the first-order correction to the parallel-flow solution. The theoretical phase information shown in figures 5 and 6 on an expanded scale (around

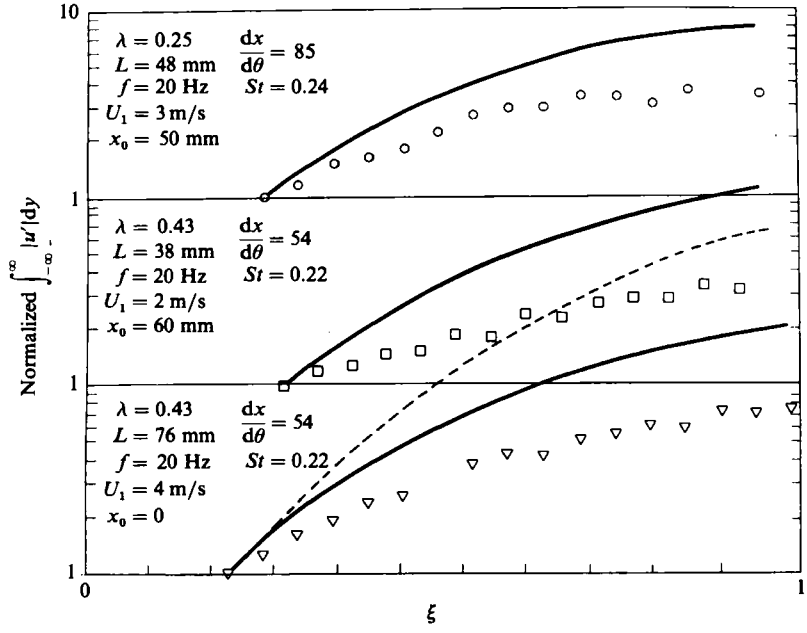

FIGURE 3. The overall amplification of disturbances with distance from the trailing edge. $St = fL/U_c$.

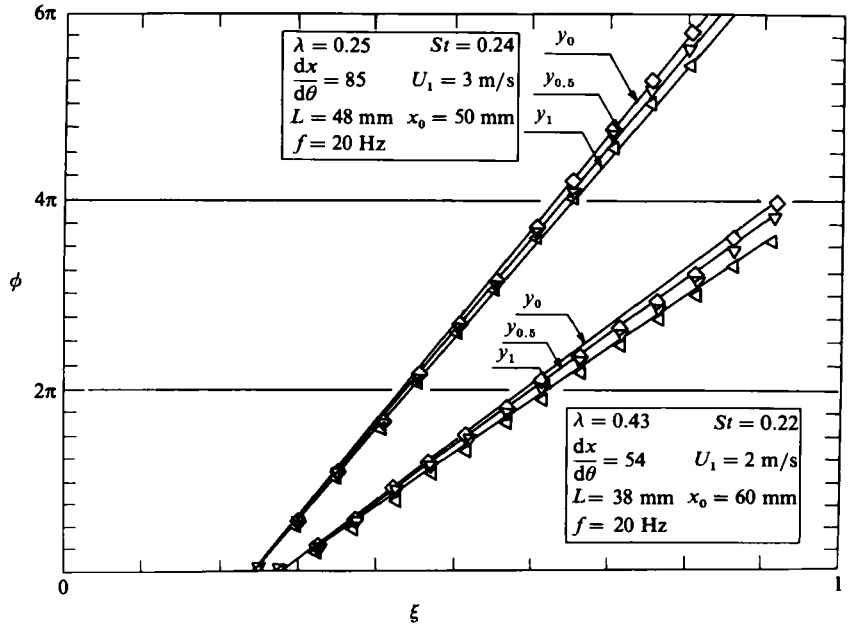

FIGURE 4. The dependence of phase on distance from the trailing edge at three lateral locations in the shear layer.

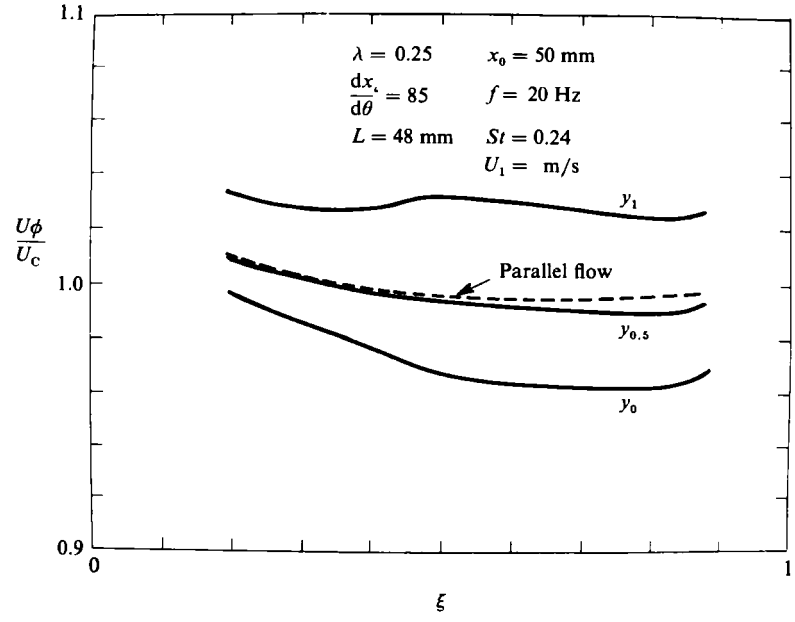

FIGURE 5. Calculated variation of phase velocity with distance from the trailing edge (corresponding to data set I).

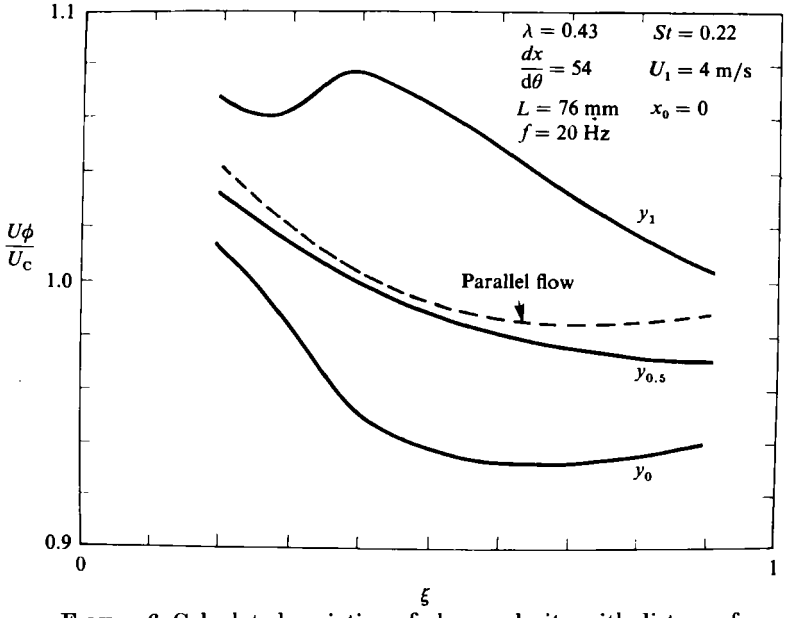

FIGURE 6. Calculated variation of phase velocity with distance from the trailing edge (corresponding to data set III).

$U_C = 0.5(\overline{U}_1 + \overline{U}_2)$) for the abovementioned rays also shows the theoretical wave speed calculated on the basis of a locally parallel mean flow. For the purpose of these calculations the integral steps across the flow had to be reduced by an order of magnitude in order to suppress spurious oscillations in the numerical solution of the phase velocity in the range $0 \leqslant \xi \leqslant 0.4$.

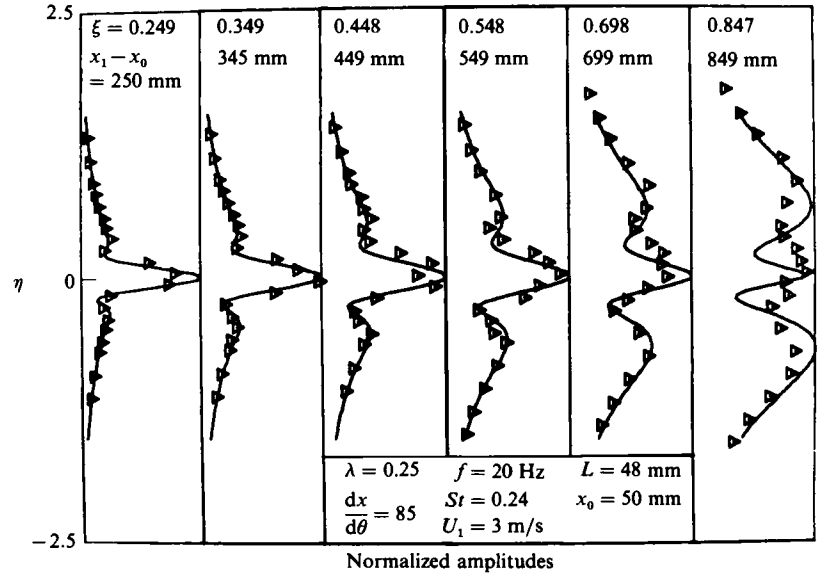

FIGURE 7. The lateral distribution of u' for the forcing frequency at various ξ-stations (data set I).

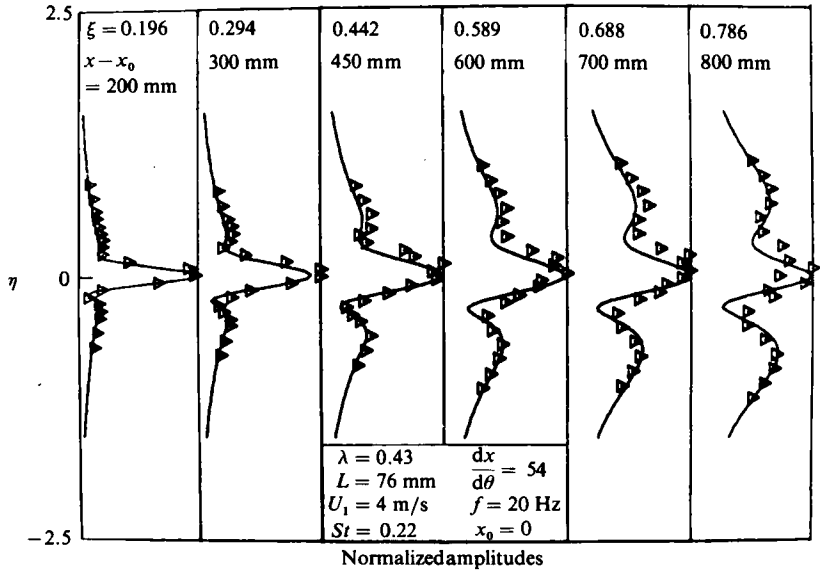

FIGURE 8. The lateral distribution of u' for the forcing frequency at various ξ-stations (data set III).

Another test of the mathematical model is provided by the amplitude and phase profiles across the mixing layer at various positions downstream from the flap. Figures 7 and 8 show the modulus of u' for the fundamental frequency at 6 stations for both experiment and theory for data sets I and III. In these figures the velocities have been normalized by equating the experimental and theoretical integrals

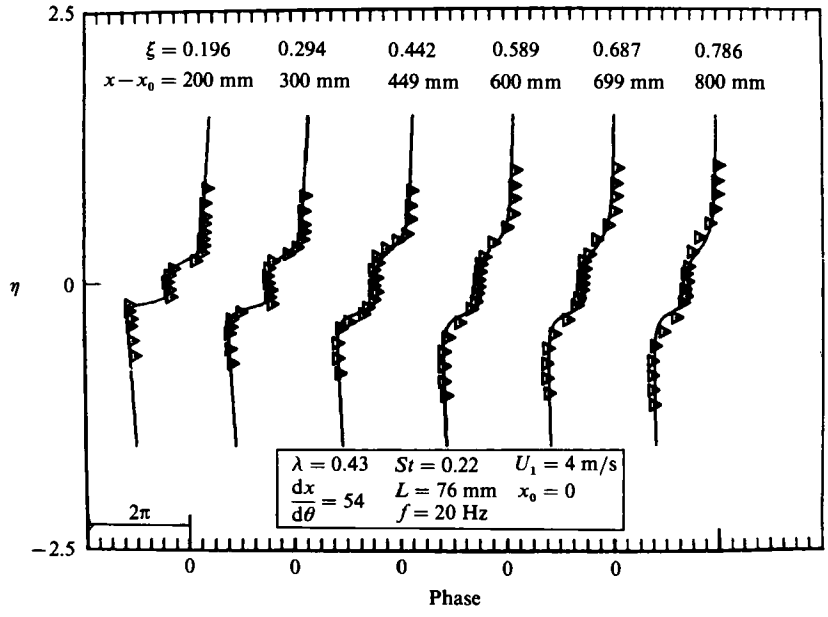

FIGURE 9. The lateral distribution of phase angles at various ξ-stations (data set III).

calculated according to (5.4). Close to the flap, a single narrow central peak in $|u'|$ is evident in both the experimental results as well as in the numerical solution. The two side lobes become progressively stronger with increasing distance from the flap, and by the end of the computational zone they become larger than the central peak. Apart from some detailed differences near the centreline, this trend is followed by the numerical solution, although correlation with experiment does not noticeably fall off far downstream. The experimental points contain far more scatter in the downstream region and this suggests that the overall flow pattern is not very steady there. Finally, the measured and computed phase profiles are compared for data set III on figure 9. The phases are shown relative to that at the centre of the mixing layer ($\eta = 0$). The agreement between the measured and computed results is really extremely good, every jump and variation being almost perfectly reflected by the theory.

6. Discussion

In this paper we are trying to examine the extent to which the large-scale vortex structure that develops in a fully turbulent mixing layer can be described by an inviscid linear model.

An 'unexcited' free mixing layer developing downstream from the trailing edge of the splitter plate will inevitably contain a large-scale oscillatory motion. The structure of the unsteady flow can be revealed through measurements of various kinds, but the overall flow pattern can often be resolved more directly with the aid of an appropriate flow-visualization technique. Apart from the fine-scale turbulence that is always present, one can then pick out the large-scale organized structures that appear in the flow. These structures appear as vortices that originate fairly close to the splitter plate. They grow as they propagate downstream, and eventually roll up

and coalesce to form larger vortices. The process appears to be closely two-dimensional, but is irregular, especially so after the first stage of vortex pairing. A very much clearer picture of the early stages of this process can be seen when the flow is artificially excited by a suitably chosen periodic disturbance, such as a trailing-edge flap. The flow then has a far more controlled behaviour, with the vortices forming and travelling downstream in a more-or-less regular manner. Again at sufficient distance from the splitter plate, the vortices will coalesce and form a new vortex pattern at the subharmonic frequency, but the process is noisy and no longer precisely locked to the motion of the flap. It turns out nevertheless that the motion under artificial excitation is reasonably representative of that in the unexcited case, except that the random element is considerably reduced.

The periodically forced case is considered in this paper, and comparisons of the observed large-scale vortex structures are made with a theoretical model of a spatially growing instability wave that is precisely periodic. Again the theoretical model is linear and inviscid, and takes no account whatsoever of the fine-scale turbulence that is present in the flow. The analysis is concerned with the prediction of the behaviour of an isolated periodic wavetrain propagating in a given mean flow. It has been assumed that the mean flow departs only slowly from a parallel-flow geometry, and that a weak modification of parallel-flow stability theory is sufficient to describe the resulting solution. In order to simplify the computations further, the mean flow was treated as a similarity flow that spreads linearly with downstream distance. This is quite a close model of the experimentally measured mean flow.

The inviscid mathematical model can only define amplified modes. If it were required to carry the calculation of a particular wavetrain through the neutral stability point, certain modifications to the equations, such as the inclusion of a small amount of viscosity, would have to be made. This was not necessary in the present exercise, where we were trying to demonstrate that a simple inviscid model was capable of describing the developing time-periodic instability of the flow within the region of amplification. The more interesting problem of a naturally excited flow, which involves the superposition of a broad band of periodic wavetrains (some of which are damped), does require some such modification. In that case the resultant solution would be expected to have a narrow spectrum such that the frequency of its peak would fall with distance from the splitter plate, because the high-frequency components become damped, whilst the waves of lowest frequency increase rapidly. It would certainly be well worth modifying the numerical procedures used here so as to compare the resulting solutions with experimental data derived from a mixing layer; first, forced by a flap driven by a pseudo-white-noise generator; and, secondly, when excited by the natural 'noise' content of the incoming turbulence. We believe that the broadband linear model would still provide a useful description of the disturbance.

The neglect of the nonlinear terms in deriving the basic perturbation equations was another very necessary simplifying assumption, but one that needs to be questioned in view of the observed amplitudes of the velocity fluctuations associated with the forced waves. Spectral analysis of the experimental axial-velocity fluctuations provide a measure of that fraction of the energy contained in a narrow band of frequencies centred on the forcing frequency (figure 10). At $\xi = 0.196$ the maximum intensity of broadband signal in the streamwise direction was equal to 0.24; some 20% of this energy fell within a narrow band around the forcing frequency. At $\xi = 0.786$ the maximum overall level of fluctuation was 0.18, corresponding to the value commonly observed in an unforced fully turbulent plane mixing layer, but here

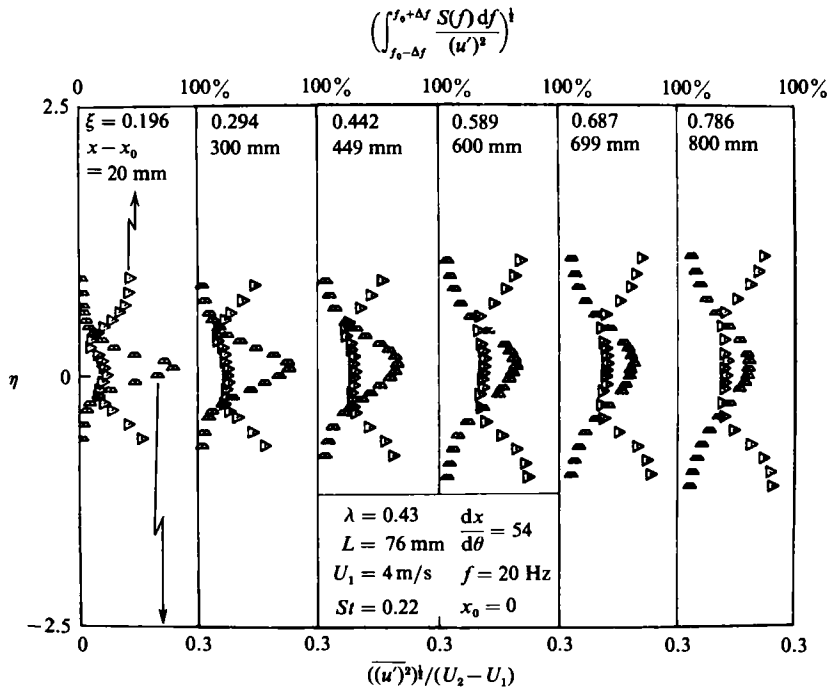

FIGURE 10. The overall turbulent intensity of the u' fluctuations and the fraction of energy contained at the forcing frequency (data set III).

45% of the energy occurred at the forcing frequency. These levels of velocity fluctuation cannot be considered as small perturbations of the mean flow, and it is not at all obvious that linearization of the equations of motion is entirely justified. Nevertheless, it turned out that the linear theory did seem capable of describing the flow surprisingly well, and this needs to be explained. Solutions of weakly nonlinear stability problems usually rely on the idea that the actual eigenfunction of the fundamental part of the motion are given by a linear calculation, and it is only through the balance of terms that an amplitude scaling is defined. It is therefore perhaps not too surprising that the details of the phase-locked velocity fluctuations are modelled quite well by the linear theory, unlike the prediction of the overall amplification, which is limited by the additional factors of dissipation and energy transfer to the fine-scale turbulence (Hussain 1983).

Another aspect of the nonlinearity concerns the determination of the mean flow. In our treatment the mean flow is assumed to be known *a priori*, whereas the nonlinear 'Reynolds stresses', arising from the unsteady flow, control the spreading rate while maintaining self-similar mean-velocity profiles. It is conceivable that the 'Reynolds stresses' could be estimated well enough from the linear calculations to provide closure, but such a calculation has not been attempted. The stability of the periodic-wave solution that has been obtained also warrants study. It may be expected that the resulting vortex pattern will be unstable to certain disturbances. This is presumably involved in vortex pairing and in the generation of subharmonic oscillations.

It is interesting to note that the present linear theory nevertheless seems to give some intimation of the vortex roll-up process. While phase velocities calculated on

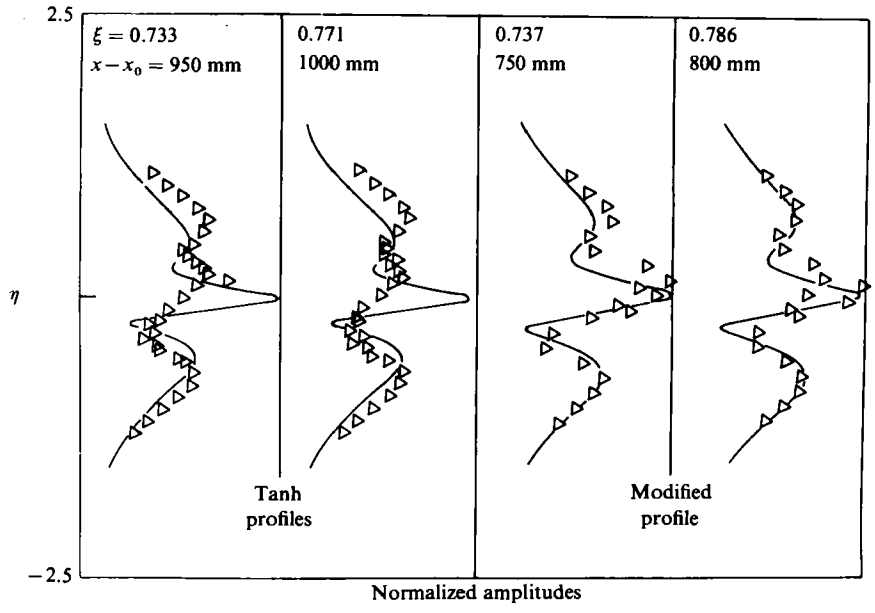

FIGURE 11. The effects of the choice of the mean-velocity profile on the predicted amplitude distribution at large distances from the trailing edge.

the basis of a parallel mean flow inevitably produce a uniform convection velocity across the shear layer, theories that take account of flow divergence do predict a variation of phase speed with location. The present computations predict that the phase advance is greater than average in the outer regions of the faster-flowing stream and lower than average in the slower-moving stream, which is in agreement with the experimental data as shown in figure 4. The faster-moving vortex structures thus appear to ride over the slower-moving ones, and are located so as to be more readily rolled up and fused into a smaller number of large vortices as in a subharmonic motion. It is worth noting further that wideband space–time correlation measurements taken in an unforced turbulent mixing layer (Oster, Wygnanski & Fiedler 1977) indicated a similar pattern of behaviour for the large-scale structures. In fact the phase velocities measured by Oster *et al.* at $\lambda = 0.43$ agree quantitatively with the present results.

Although the velocity-profile shape used in the present computations differed only slightly from the 'tanh' profile that has traditionally been used in mixing-layer stability work, this has had significant effect on the detail of the theoretical predictions. Close to the trailing edge of the splitter plate, where the mixing layer is thin compared with the wavelength of an instability mode, the behaviour of the perturbation is controlled solely by the velocities of the two streams. Farther downstream the mixing layer becomes thicker, and, when it has a dimension commensurate with the wavelength, details of the profile shape become important.

Then the predicted amplification rates and the amplitude distribution of the fluctuations are influenced by the actual shape of the profile, and in particular by the curvature. In figure 11, the amplitude distribution predicted by using the 'tanh' profile is compared with the amplitude distribution using the modified profile (5.2) at approximately the same dimensionless computational coordinate. The results obtained from the modified profile agree much better with experiment at the stations

indicated in the figure, because the shape of the velocity profiles affects the constants C_0 and C_1 (determined in (3.2) and (5.3) respectively) and therefore the ratio between the physical and computational distances. The use of the 'tanh' profile in the theoretical model required comparison with experimentally obtained perturbation profiles at stations farther downstream (for the same dimensionless coordinate ξ), by which point the agreement with the computed eigenfunctions was poor. The different profile shapes also cause differences in the overall amplification as exemplified in figure 3, where at the end of the computational zone the perturbation associated with the tanh profile had undergone an amplification which is 3.5 times larger than the corresponding amplification of the modified profile (data set III).

7. Conclusions

The large-scale vortex structures that occur in a forced mixing layer have been modelled by a linear inviscid stability theory. Experimental measurements showed that the mean flow in the region considered conformed well to a similarity model having a velocity profile close to, but not identical with, the 'tanh' shape. The thickness of the mixing layer was found to increase almost linearly with distance from some origin close to the trailing edge of the splitter plate. The velocities associated with the large-scale organized structures were measured and compared with the distribution predicted by the theory. Comparisons of both the magnitude and phase of the velocity fluctuations across various sections of the flow showed remarkable agreement. The overall integrated behaviour involving the amplification along the mixing layer compared less favourably with the theoretical calculations, and this may have been due to the neglect of the nonlinear terms.

The authors wish to thank Professor E. Reshotko for reading and commenting on the manuscript. This research was supported in part by the U.S. Air Force Office of Scientific Research under grant 77-3275.

REFERENCES

Bouthier, M. 1972 *J. Méc.* **11**, 599.

Bouthier, M. 1973 *J. Méc.* **12**, 75.

Crighton, D. G. & Gaster, M. 1976 *J. Fluid Mech.* **77**, 397.

Crow, S. C. & Champagne, F. H. 1971 *J. Fluid Mech.* **48**, 547.

Fiedler, H. E., Dziomba, B., Mensing, P. & Rosgen, T. 1981 In *The Role of Coherent Structures in Modelling Turbulence and Mixing* (ed. J. Jimenez). Lecture Notes in Physics, vol. 136, p. 219. Springer.

Freymuth, P. 1966 *J. Fluid Mech.* **25**, 683.

Gaster, M. 1974 *J. Fluid Mech.* **66**, 465.

Gaster, M. 1981 In *Transition and Turbulence* (ed. R. E. Meyer). Academic.

Ho, C. M. 1981 In *Numerical and Physical Aspects of Aerodynamic Flows* (ed. T. Cebeci), p. 521. Springer.

Hussain, A. K. M. F. 1983 *Phys. Fluids* **26**, 2816.

Hussain, A. K. M. F. & Reynolds, W. C. 1970 *J. Fluid Mech.* **41**, 241.

Landahl, M. T. 1967 *J. Fluid Mech.* **29**, 441.

Liu, J. T. C. & Merkine, L. 1976 *Proc. R. Soc. Lond.* A **352**, 213.

Malkus, W. V. R. 1956 *J. Fluid Mech.* **1**, 521.

Michalke, A. 1964 *J. Fluid Mech.* **19**, 543.

MICHALKE, A. 1965 *J. Fluid Mech.* **23**, 521.

MONKEWITZ, P. A. & HUERRE, P. 1982 *Phys. Fluids* **25**, 1137.

OSTER, D. & WYGNANSKI, I. 1983 *J. Fluid Mech.* **123**, 91.

OSTER, D., WYGNANSKI, I. & FIEDLER, H. 1977 In *Turblence in Internal Flows* (ed. S. N. B. Murthy), p. 67. Hemisphere.

SCHUBAUER, B. & SKRAMSTAD, H. K. 1949 *NACA Rep.* 909.